

Simple stellar population models including blue stragglers

Yu Xin,^{1*} Licai Deng,² Richard de Grijs³ and Pavel Kroupa¹

¹*Argelander-Institut für Astronomie (Sternwarte), Universität Bonn, Auf dem Hügel 71, D-53121 Bonn, Germany*

²*Key laboratory for optical astronomy, National Astronomical Observatories, Chinese Academy of Sciences, Beijing 100012, China*

³*Kavli Institute for Astronomy and Astrophysics, Peking University, Beijing 100871, China*

Accepted —. Received —; in original form —

ABSTRACT

Observations show that nearly all star clusters and stellar populations contain blue straggler stars (BSs). BSs in a cluster can significantly enhance the integrated spectrum of the host population, preferentially at short wavelengths, and render it much bluer in photometric colours. Current theoretical simple stellar population (SSP) models constructed within the traditional framework of single and binary stellar evolution cannot fully account for the impact of these objects on the integrated spectral properties of stellar populations. Using conventional SSP models without taking into account BS contributions may significantly underestimate a cluster’s age and/or metallicity, simply because one has to balance the observed bluer colours (or a bluer spectrum) with a younger age and/or a lower metallicity. Therefore, inclusion of BS contributions in SSP models is an important and necessary improvement for population synthesis and its applications. Here, we present a new set of SSP models, which include BS contributions based on our analysis of individual star clusters. The models cover the wavelength range from 91 Å to 160 μm, ages from 0.1 to 20 Gyr and metallicities $Z = 0.0004, 0.004, 0.008, 0.02$ (solar) and 0.05. We use the observed integrated spectra of several Magellanic Cloud star clusters to cross-check and validate our models. The results show that the age predictions from our models are closer to those from isochrone fitting in the clusters’ colour-magnitude diagrams compared to age predictions based on standard SSP models.

Key words: blue stragglers – galaxies: star clusters – Magellanic Clouds.

1 INTRODUCTION

Evolutionary population synthesis (EPS) has been widely used as a powerful tool to study the stellar contents of galaxies. In essence, EPS compares the observed, integrated spectrum of a galaxy with a combination of spectra of simple stellar populations (SSPs; single-age, single-metallicity populations) of different ages and metallicities to infer the galaxy’s star-formation history. Over the past two decades, much work has been done to improve the accuracy of EPS and SSP models in various contexts (e.g., Bica & Alloin 1986; Fritzev, Alvensleben & Gerhard 1994; Worthey 1994; Leitherer et al. 1999; Vazdekis 1999; Bruzual & Charlot 2003, hereafter BC03; Thomas et al. 2003). Unfortunately, population synthesis models still suffer from a number of limitations. One is our poor understanding of some advanced single-star evolutionary phases, such as of supergiants and asymptotic-giant-branch (AGB) stars (Yi 2003), while a second is an absence in the models of the results of stellar interactions,

such as the so-called ‘stragglers’ formed through mass transfer in binaries or stellar collisions. Such stars are usually very bright and can strongly affect the integrated-light properties of the entire system. The potential uncertainties inherent to EPS caused by ignoring these components could be much larger than those still remaining and due to the variety of input physics among different models.

In this paper, we focus on the second limitation to the standard SSP models. We present a new set of SSP models which include contributions from blue straggler stars (BSs).

BSs are common and easily identified in colour-magnitude diagrams (CMDs) of star clusters. They are members of the host cluster and located above and blueward of the cluster’s main-sequence (MS) turnoff. The standard theory of single-star evolution cannot explain the presence of BSs in SSP CMDs, and thus the standard SSP models do not include contributions of BSs. All currently accepted scenarios of BS formation are related to stellar interactions. Coalescence in primordial binaries can launch BSs to positions up to 2.5 magnitudes brighter than the MS turnoff (McCrea 1964). Mergers of binary-binary systems can produce possible BSs with masses four times those of stars at

* YX is supported by the Alexander von Humboldt Foundation.
E-mail: yxin@astro.uni-bonn.de

Table 1. Fundamental ingredients of the BS-SSP models.

Name	Property	Source
Padova1994 isochrones	$Z=0.0001-0.05$ Age=4Myr–20Gyr	Bertelli et al. (1994)
BaSeL spectral library	91Å–160 μ m median resolution $\lambda/\Delta\lambda \approx 300$	Lejeune et al. (1997)
Initial mass function	$\xi(\log m) \propto m^{-1.35}$ table 1 in Chabrier (2003)	Salpeter IMF (Salpeter 1955) Canonical IMF (Kroupa 2001, 2002; Chabrier 2003)

the MS turnoff (Leonard & Linnell 1992). Stellar collisions are also an important formation channel of BS formation in globular clusters (GCs) and open clusters (OCs; Glebbeek et al. 2008). Given the high luminosities and common presence of BSs in stellar systems (e.g., Ahumada & Lapasset 1995 for OCs; Piotto et al. 2002 for GCs; Mapelli et al. 2009 for dwarf galaxies), we believe that we must consider the effects of BSs in studies of stellar populations using population synthesis applied to unresolved observations. The key issue is how to accurately include BS contributions in SSP models.

Studies show that no single mechanism can account for the entire BS population observed in any one star cluster (Stryker 1993). This means that it is not easy to theoretically measure the respective contribution of BSs in SSPs of different ages and metallicities. Therefore, building up BS population characteristics empirically from the statistics of a large sample of star clusters could be more practical and reliable than relying on incomplete theoretical approaches. This way, the behaviour of BSs (in terms of their specific frequency and relative distribution with respect to the MS turnoff in CMDs) can be modelled. OCs in the Galaxy have a number of advantages for use as a working sample, for instance, (i) they are good observational templates of ideal SSPs in the real world, and all BSs in a given OC belong to a single population; (ii) many OCs have multi-epoch proper-motion and/or radial-velocity data, so that their cluster membership probabilities can be measured accurately.

Preliminary modelling of BS effects has been done on the basis of individual clusters in our previous papers (Deng et al. 1999; Xin & Deng 2005; Xin et al. 2007, 2008), where we (i) introduced the method used for calculating the realistic, integrated spectrum of a star cluster including the contribution of BSs; (ii) analysed the modifications to the integrated spectra and broad-band colours caused by BSs; and (iii) estimated the possible uncertainties in the conventional SSP models, showing that the ages of star clusters can be underestimated by up to 50% if BS contributions are not considered.

In this paper, we present a set of BS-SSP models based on a statistical study of Galactic OCs. A working sample including 100 Galactic OCs is used to reduce stochastic effects in collecting the required statistical relations. We also use the standard deviation (σ) to keep the statistics in a relatively small dispersion region. Our models cover the wavelength range from 91 Å to 160 μ m, ages from 0.1 to 20 Gyr and metallicities $Z = 0.0004, 0.004, 0.008, 0.02$ (solar metallicity) and 0.05.

This paper is organised as follows. In Section 2, we present the statistical results of the properties of BS populations based on 100 Galactic OCs. Here, we also describe

the construction procedure of our models. In Section 3, we discuss our model results and compare them with those of BC03. In Section 4, we test our models by comparison with the broad-band colours of OCs. Our model colours are in good agreement with observed OC colours (which include BS contributions). In Section 5, we test our models using observed integrated spectra of star clusters. Compared to BC03, our models yield more accurate age predictions at a range of wavelengths, including in the optical regime. Finally, a summary and further brief discussion is contained in Section 6.

2 BS-SSP MODELS

The fundamental ingredients of our models are listed in Table 1. For convenience, we use the widely adopted BC03 models as reference. Modifications owing to BSs are calculated as increments to the BC03 SSPs of the same age and metallicity. We adopted the Padova1994 isochrones (Bertelli et al. 1994) and the BaSeL spectral library (Lejeune et al. 1997) because they homogeneously cover the widest ranges of age and metallicity, and the longest wavelength range. The Padova2000 isochrones (Girardi et al. 2000) are based on a more recent equation of state and low-temperature opacities compared to Padova1994. However, we decided against adopting them for our model construction, because BC03 do not recommend to use their SSPs based on the Padova2000 isochrones. They state that their models based on the Padova2000 isochrones “tend to produce worse agreement with observed galaxy colours” (BC03, their footnote 6). High-resolution observational spectral libraries (e.g., Pickles et al. 1998; Le Borgne et al. 2003) suffer from problems related to limited parameter coverage. Instead of combining spectra from different libraries to enlarge our parameter coverage, we decided to use only the theoretical library.

For consistency with BC03, we adopted the Salpeter and Chabrier stellar initial mass functions (IMFs; Salpeter 1955; Chabrier 2003). As clearly shown by Dabringhausen et al. (2008, their fig. 8), the Chabrier IMF is almost indistinguishable from the Kroupa IMF (Kroupa 2001, 2002) when normalised as $\int_{0.1}^{100} \xi(m) dm = 1M_{\odot}$, which is exactly how both BC03 and we ourselves normalise the SSP models. Using such a normalisation, the slight differences between the two IMFs cannot cause any effective modifications as regards the BS contribution to SSPs. Therefore, we refer to the IMF (in addition to the Salpeter IMF) as the ‘Canonical IMF’ throughout this work. It can be conveniently described by a two-part power law, $\xi(m) \propto m^{-\alpha_i}$, with $\alpha_1 = 1.3$ for the stellar-mass range $0.08 \leq m/M_{\odot} < 0.5$ and $\alpha_2 = 2.3$ for

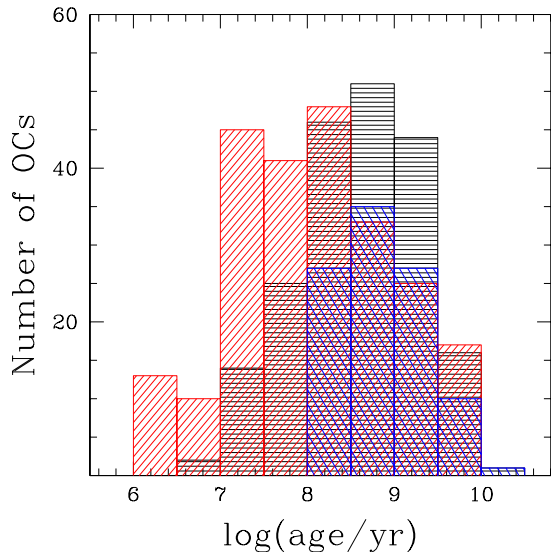


Figure 1. Number distributions of Galactic OCs containing BSs as a function of age. Horizontal shading represents the statistics from the Ahumada & Lapasset (2007) catalogue. The hatching from the bottom left to the top right represents the statistics from the Ahumada & Lapasset (1995) catalogue, while that from the top left to the bottom right shows the number distribution of our working sample (100 Galactic OCs).

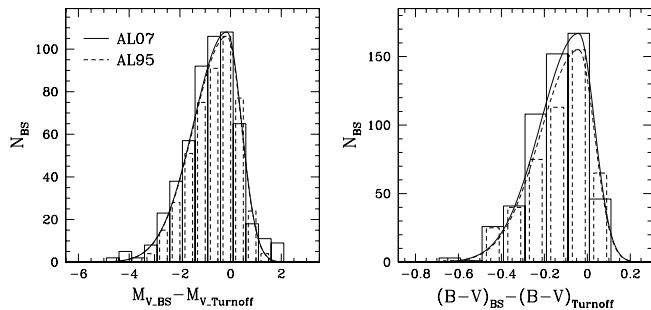


Figure 2. BS distribution functions in the CMD versus M_V (left panel) and $(B - V)$ (right panel). The solid histograms represent the statistics from the AL07 catalogue, and the solid curves are the corresponding Gaussian approximations to either side of the peak. The dashed histograms and dashed curves are the results from the AL95 catalogue. The statistics are processed based on the photometric data of BSs in 33 OCs of age ≥ 1.0 Gyr and common to all of AL95, AL07 and our working sample.

$m \geq 0.5M_{\odot}$ (Kroupa 2001), or in terms of a power law plus a lognormal form as presented in table 1 of Chabrier (2003).

2.1 BS statistics

Basically, two properties of BS populations are relevant to the modelling of BS behaviour in SSPs, i.e., the number of BSs (N_{BS}) in the SSP and their distribution in the SSP’s CMD. In this paper, both properties are obtained empirically from the observed OC CMDs. A working sample including 100 Galactic OCs from the catalogue of Ahumada

& Lapasset (1995, hereafter AL95) is adopted to secure the reliability of the statistical results.

Fig. 1 shows the differences among the number distributions of OCs containing BSs versus age for the Ahumada & Lapasset (2007, hereafter AL07) catalogue (horizontal hatching), the AL95 catalogue (slanted hatching from bottom left to top right) and our sample (slanted hatching from top left to bottom right). AL95 and AL07 published the most complete catalogues to date in terms of photometric data of BSs in Galactic OCs. They include almost all OCs containing BSs in the solar neighbourhood. In particular, they also include the so-called ‘yellow stragglers’ (e.g., Portegies Zwart et al. 1997; Deng et al. 1999, their fig. 1) in their BS catalogues. Yellow stragglers are located between the MS turnoff and the giant branch in CMDs (i.e., they are redder than BSs), therefore adding extra light preferentially in the optical spectral regions of a cluster.

Fig. 1 shows that, compared to AL95, AL07 dramatically reduced the number of young OCs containing BSs, mainly because of the difficulty of identifying BSs in the CMD of a star cluster that does not exhibit at least a fully developed red-giant-branch (RGB) phase (particularly when membership-probability information is lacking). Moreover, most of the BSs in young OCs (i.e., $\log(\text{age}/\text{yr}) < 8.0$ in this paper) from both catalogues are located close to the MS turnoff point in the CMD, which means that it is hard to distinguish BSs from MS stars. Such BSs cannot effectively modify the spectral intensity of a cluster. Therefore, we start the selection of our working sample based on OCs with $\log(\text{age}/\text{yr}) \geq 8.0$.

Meanwhile, to construct a spectrum of the BS population for a given OC, we need to obtain the physical parameters of the BSs in the CMD of the OC (see also Section 2.2). To do this, we need the age, metallicity, colour excess and distance modulus for each OC, which are not all included in either AL95 or AL07. Therefore, we decided to keep only the photometric data of BSs from AL95, to ensure a homogeneous selection of the BS sample. We collected the remaining OC parameters from the recent literature (see Xin et al. 2007, their table 1). In practice, OCs with $\log(\text{age}/\text{yr}) \geq 8.0$ from AL95 are included as sample clusters if reliable parameters can be found, in the sense that most of the BSs are located at reasonable positions in the CMD with respect to the Padova1994 isochrone for the OC’s age and metallicity.

There are 33 OCs with age ≥ 1.0 Gyr in the combined catalogue comprised of AL95, AL07 and our working sample. Older OCs have better statistics as regards their BS populations. Using the photometric data of the BSs in these 33 OCs as an example, we show the BS distribution functions versus the MS turnoff point in Fig. 2, as a function of M_V (left panel) and $(B - V)$ (right panel). We use this figure to detect differences in the BS distributions in the CMD between the AL95 and AL07 statistics. The solid histograms represent the statistics from the AL07 catalogue, and the solid curves are the corresponding Gaussian approximations to either side of the peak. The dashed histograms and dashed curves are the results from the AL95 catalogue. The same technique is used to construct the BS distribution functions in the CMD for our model construction (see below). Based on Fig. 2, the distribution functions of both M_V and $(B - V)$ do not exhibit any essential differences between the AL95 and the AL07 catalogues. Therefore, we continue

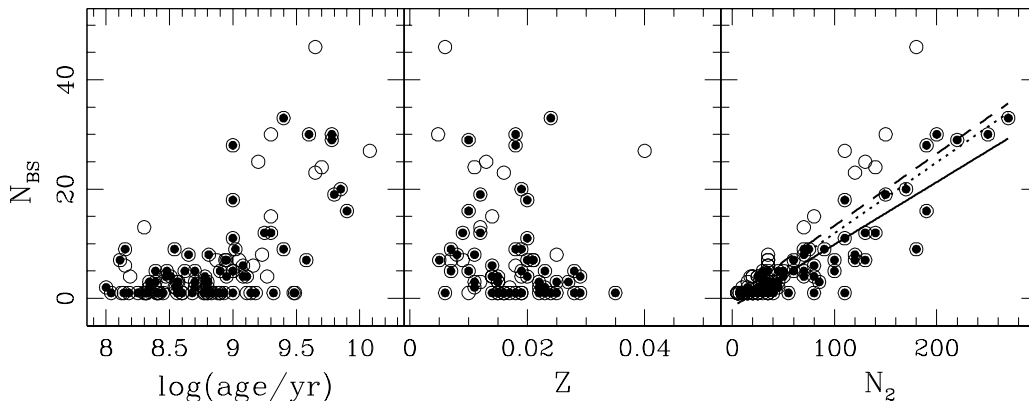


Figure 3. Correlations (if any) between N_{BS} and the age, metallicity and richness (N_2) of Galactic OCs, respectively. The open circles show the results for the 100 OCs in our working sample. The filled circles mark the OCs with N_{BS}/N_2 less than the average ratio plus 1σ (standard deviation). The solid line in the right-hand panel is the least-squares fit to the filled circles; it is given by Eq. (1). For reference, the dotted line in the right-hand panel is the least-squares fit to all OCs (open circles), and the dashed line is the fit to OCs with ages ≥ 1.0 Gyr.

on the basis of the results from our previous work, i.e., the parameters of the sample clusters and the BS population from AL95. Details of the BS properties are presented in Figs. 3–5. Fig. 3 shows N_{BS} as a function of the age, metallicity and richness of the sample OCs. The richness of a star cluster is represented by N_2 , which is the number of cluster member stars within 2 magnitudes below the cluster’s MS turnoff. The open circles represent the results for the 100 Galactic OCs. Because of the small number of member stars and even smaller number of BSs in the individual OCs, the results directly derived from Fig. 3 are very stochastic, and thus we use the ratio of N_{BS}/N_2 to reduce the effects of stochasticity. We use this ratio as definition of the specific frequency of BS components in SSPs. We calculated the standard deviation (σ) of the ratio for the entire sample,

i.e., $\sigma = \sqrt{\frac{\sum_{i=1}^N (\frac{N_{\text{BS}}}{N_2}_i - \frac{N_{\text{BS}}}{N_2})^2}{N \times (N-1)}}$ and $N = 100$. We marked the OCs with $\frac{N_{\text{BS}}}{N_2} \leq \frac{N_{\text{BS}}}{N_2} + 1\sigma$ with filled circles in Fig. 3.

The left-hand panel in Fig. 3 shows N_{BS} versus cluster age on a logarithmic scale. N_{BS} seems largely insensitive to age until a sudden increase for ages greater than 1.0 Gyr. Based on this figure it is hard to discern any correlation between the two parameters, and it is also risky to jump to the conclusion that N_{BS} is not correlated with age. The seemingly constant N_{BS} for age < 1.0 Gyr could be caused by the confusion of defining an accurate MS turnoff point and a BS population in relatively young star clusters. In our model construction, we have not adopted any correlation between N_{BS} and age. The only correlation we used is that between N_{BS} and N_2 (shown in the right-hand panel in Fig. 3; see below). In fact, for SSPs, N_{BS} and age are related through the SSP’s N_2 . N_2 increases following the IMF slope as the SSP ages, and so does N_{BS} through the correlation between N_{BS} and N_2 .

The middle panel of Fig. 3 shows N_{BS} as a function of metallicity for our sample OCs with published metallicity in-

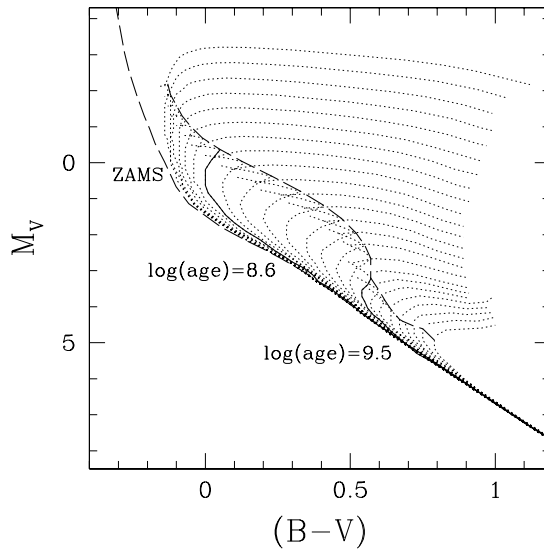


Figure 4. Criteria used for our age-bin selection. The dotted lines are the isochrones for ages between 0.1 and 20 Gyr, truncated at the bottom of the RGB phase. The two dashed lines mark the boundaries of the MS stage. The choice of age bin is shown as the solid lines.

formation. No correlation can be established. We previously studied whether the BS strengths are sensitive to metallicity. We did not find any obvious correlation between these two parameters either (Xin & Deng 2005, their fig. 18).

The right-hand panel of Fig. 3 clearly shows that only N_{BS} and N_2 are correlated. The implication of this correlation is that N_{BS} is proportional to the richness of an SSP, but not (at least not obviously) to any other parameter, such as age or metallicity. The solid line in the right-hand panel

Table 2. Gaussian-profile parameters for BS distribution functions in different age bins.

Age bin (yr)	bin size (mag)	μ (mag)	$f^-(x)$			$f^+(x)$		
			σ	x range	σ	x range		
$8.0 \leq \log(\text{age}/\text{yr}) \leq 8.6$	M_V	0.45	0.26	0.9454 ± 0.0126	$[-3.00, 0.26]$	0.4056 ± 0.0451	$[0.26, 1.65]$	
	$(B - V)$	0.03	-0.01	0.0563 ± 0.0084	$[-0.19, -0.01]$	0.0418 ± 0.0027	$[-0.01, 0.12]$	
$8.6 < \log(\text{age}/\text{yr}) \leq 9.5$	M_V	0.40	0.112	1.0464 ± 0.1299	$[-3.50, 0.112]$	0.5470 ± 0.0532	$[0.112, 2.00]$	
	$(B - V)$	0.075	-0.005	0.1544 ± 0.0109	$[-0.530, -0.005]$	0.0678 ± 0.0079	$[-0.005, 0.220]$	
$\log(\text{age}/\text{yr}) > 9.5$	M_V	0.55	-1.08	0.8155 ± 0.0289	$[-3.83, -1.08]$	0.6711 ± 0.1931	$[-1.08, 1.20]$	
	$(B - V)$	0.08	-0.06	0.1472 ± 0.0080	$[-0.55, -0.06]$	0.0837 ± 0.0161	$[-0.06, 0.20]$	

is the least-squares fit to the filled circles. For reference, we present two more fits for different samples. The dotted line is the least-squares fit to all OCs (open circles), while the dashed line is the fit to those OCs that are older than 1.0 Gyr. It is hard to tell which fit is the most accurate. We choose the solid line for estimating N_{BS} in an SSP simply to avoid exaggeration of the BS-enhanced intensity in our SSPs. The correlation can be empirically described as

$$N_{\text{BS}} = (0.114 \pm 0.006) \times N_2 - (1.549 \pm 0.731). \quad (1)$$

The uncertainties in the coefficients result from the 1σ uncertainty in N_{BS}/N_2 .

The loci of BSs in cluster CMDs are fixed by their formation and evolutionary processes (Ferraro et al. 2009), which could still be stochastic owing to the varying physical conditions among star clusters. Thus, it is impossible to construct the specific distribution function of the BS population for each individual SSP. A feasible approach to generate a BS population in the CMD is to work out a uniform BS distribution function.

The dotted lines in Fig. 4 are isochrones with ages between 0.1 and 20 Gyr, truncated at the bottom of the RGB phase. The two dashed lines, i.e., the zero-age MS (ZAMS) and the boundary between the MS and post-MS phases, highlight the entire MS stage for all isochrones. The distance between the two dashed lines becomes narrower in the colour range in the CMD for older – $\log(\text{age}/\text{yr}) \geq 9.5$ – and younger – $\log(\text{age}/\text{yr}) \leq 8.6$ – SSPs, which means that a uniform BS distribution function will certainly push a BS population towards red colours for SSPs with a MS turnoff close to the ZAMS. To avoid uncertainties associated with the distance between the MS turnoff points and the ZAMS, we consider BS distribution functions in three different age bins, i.e., $8.0 \leq \log(\text{age}/\text{yr}) \leq 8.6$, $8.6 < \log(\text{age}/\text{yr}) \leq 9.5$, and $\log(\text{age}/\text{yr}) > 9.5$. The solid lines in the figure show the age-bin selection.

Since the bin selection is done empirically, we tested that a small change in the age-bin selection, i.e., $\Delta \log(\text{age}/\text{yr}) = 0.1$, cannot effectively modify the BS distribution in the CMDs and, consequently, affect our model results. Specifically, we construct the BS distribution functions with $\log(\text{age}/\text{yr}) = 8.6$ included in the older age bin and calculate the $(U - B)$ and $(B - V)$ colours of the SSP with $Z = 0.02$ and $\log(\text{age}/\text{yr}) = 8.6$. The colour changes resulting from adopting different distribution functions are < 0.0001 mag for both colours. The same result is found for a test with $\log(\text{age}/\text{yr}) = 9.5$.

We align the MS turnoff points of all OCs in our working

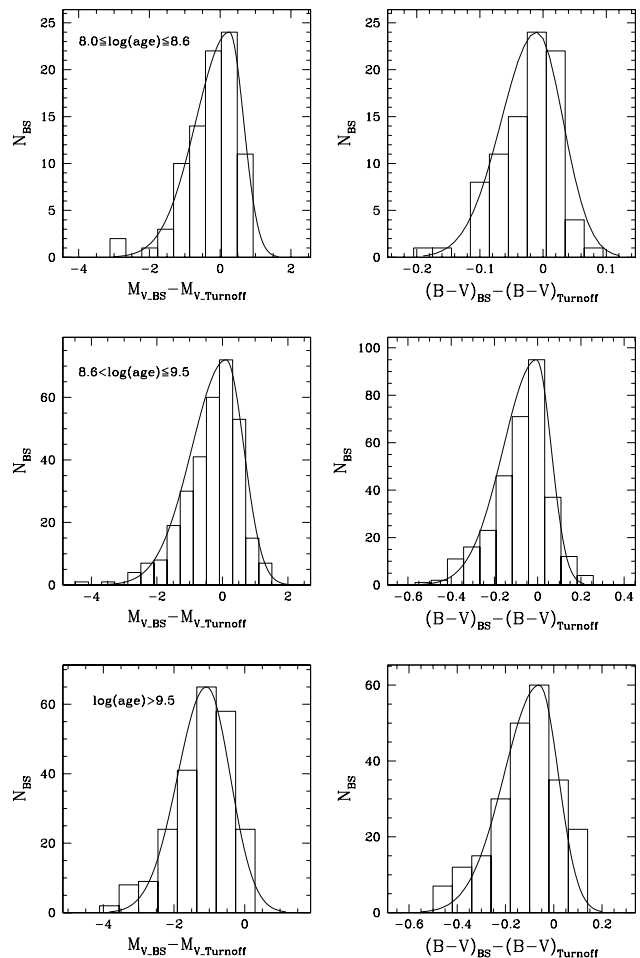


Figure 5. BS distribution functions in our OC CMDs in three different age bins as a function of M_V (left panels) and the $(B - V)$ (right panels). In each panel, a Gaussian profile is used to describe either side of the peak separately.

sample to obtain a sufficient number of BSs for good statistics. Fig. 5 shows the distribution functions of BSs versus the MS turnoff point in three different age bins as a function of M_V (left panels) and $(B - V)$ (right panels). For each of the distributions, a Gaussian profile is adopted to fit either side of the peak separately, based on which we construct the BS population in the CMD of an SSP using Monte Carlo simu-

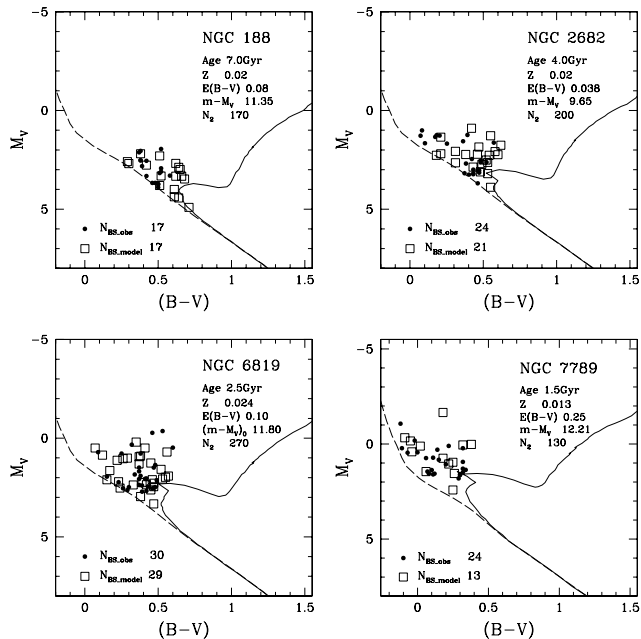


Figure 6. Comparison between the observed and modelled BS populations in the CMDs of four representative Galactic OCs. In each panel, the fundamental cluster parameters are given in the top right-hand corner, the solid curve is the isochrone representing the cluster’s age and metallicity, the dashed line is the zero-age MS, the solid circles are the observed BSs from AL95, and the open squares are the model BSs based on Monte Carlo simulations. $N_{\text{BS_model}}$ is calculated using the observed value of N_2 in Eq. (1).

lations in two dimensions (M_V and $(B-V)$). All Gaussian profiles have the same standard format,

$$f(x) = \exp\left[-\frac{(x-\mu)^2}{2\sigma^2}\right], \quad (2)$$

where μ is the peak position and σ the standard deviation. The notation $x = \Delta M_V = M_{V_{\text{BS}}} - M_{V_{\text{TO}}}$ refers to the increment in luminosity (M_V) of a BS with respect to the SSP’s turnoff luminosity; $x = \Delta(B-V) = (B-V)_{\text{BS}} - (B-V)_{\text{TO}}$ is the equivalent increment in colour index ($B-V$). The specific values of μ and σ for different x ranges are listed in Table 2. Here, $f^-(x)$ and $f^+(x)$ refer to the left- and right-hand sides of the Gaussian profiles, respectively.

Since the distribution functions are constructed empirically from observational statistics, the values of both μ and σ are inevitably sensitive to the selection of the bin size. To find reasonable descriptions for the Gaussian profiles, we start exploring the statistics of M_V and $(B-V)$ in each age bin with a bin size of $\Delta M_V = 0.20$ and $\Delta(B-V) = 0.010$ mag, and we subsequently increase the bin size in steps of $\Delta M_V = 0.05$ and $\Delta(B-V) = 0.005$ mag until the distribution resembles a Gaussian function. The adopted bin sizes for ΔM_V and $\Delta(B-V)$ for each age bin are given in column (3) of Table 2. The μ and σ values listed in the table are calculated based on the corresponding bin size.

In addition to the distribution function, a further boundary that also constrains BS positions in the CMD is the ZAMS. Any BSs located beyond the ZAMS, i.e., with

bluer colours than the ZAMS for the same luminosity, will not be generated by our program. This assumption is made mainly because we treat BSs as MS stars and describe them using standard MS models.

2.2 Model construction

Our sample of 100 Galactic OCs has limited parameter coverage in age and metallicity, i.e., it covers ages from 0.1 to 12 Gyr and metallicities from $Z = 0.0048$ to 0.035 (Xin et al. 2007, their table 1). To consider the BS contributions for the full set of SSP models, some extrapolations of the parameter space have been adopted based on the results from OCs and some reliable working assumptions: (i) ages from 0.1 to 20 Gyr, with the lower limit set by the difficulty to identify BS components in star clusters younger than 100 Myr, while the BS properties are not expected to change dramatically in very old stellar populations (see Section 3); and (ii) metallicities $Z = 0.0004, 0.004, 0.008, 0.02$ and 0.05. Although the current best constraint on the age of the Universe is 13.73 ± 0.12 Gyr from the WMAP measurements, we retain an age of 20 Gyr¹ as upper age limit of the models, both to keep the model grids the same as those of BC03, and to enable the applications of the models to the studies of stellar populations if a possible correction to the currently accepted cosmology is required. We extend the metallicity to a lower boundary of $Z = 0.0004$ and a maximum value of $Z = 0.05$ because the statistics of OCs show that BS behaviour is not sensitive to metallicity. ($Z = 0.0001$ is not included in the models because HB stars, instead of BSs, dominate the energy in the ultraviolet and blue bands in extremely metal-poor populations.)

Our construction procedure for SSP models including BS contributions is summarised as follows. (i) We use the standard models (we use BC03 in this paper, but we can in principle use any other SSP flavour as well) to represent the integrated spectrum of the ‘normal’ SSP member stars. We subsequently use the statistical properties of BSs from Galactic OCs to generate the BS population for the appropriate SSP. (ii) We calculate the spectrum of the BS population and combine it with the spectrum of the normal member stars after the appropriate flux calibration. The composite spectrum is the integrated spectrum of the BS-corrected SSP.

In detail, the model construction includes the following steps.

- (1) We assume that any given model SSP contains

¹ The BC03 SSP models and the stellar evolutionary tracks that form their basis have been calculated for ages up to 20 Gyr. It is not straightforward to correct this to a lower age; one would need to recalculate all stellar evolutionary tracks for all metallicities and, for instance, update the precise descriptions of opacities, convection, and evolution of, e.g., horizontal branch (HB) and AGB stars. This situation is worsened by the fact that young OCs, up to ~ 5 Gyr, have been used to properly and robustly constrain stellar evolution at younger ages, whilst at older ages the observational diagnostics are less sensitive to changes in age, resulting in significantly greater uncertainties at those ages. These are therefore issues that one needs to keep in mind in the context of physical parameters derived for older GCs using both the BC03 and our models.

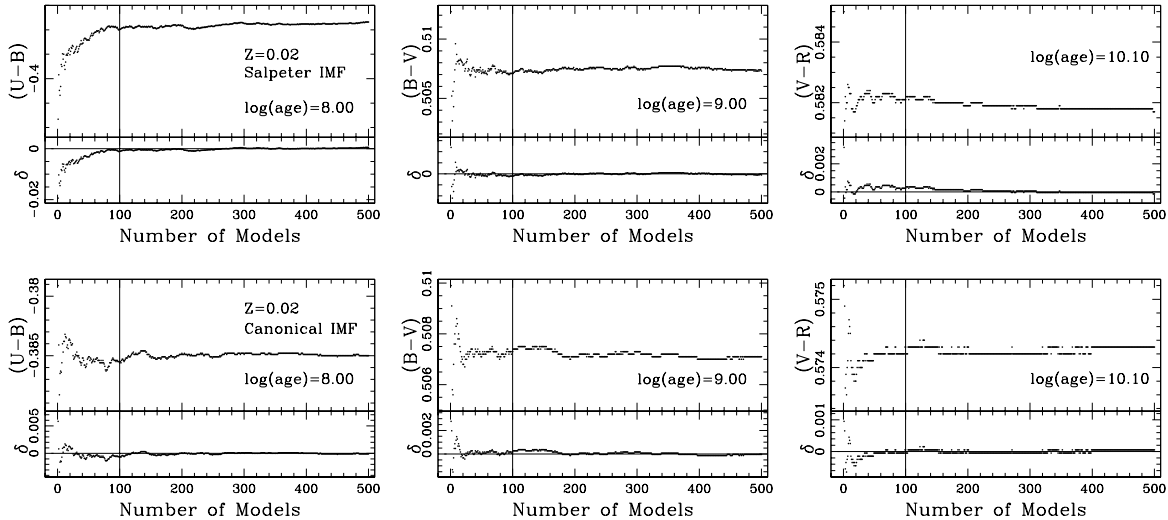


Figure 7. Choice of the number of models to calculate the spectrum of the BS population in our model construction (see Section 2.2). Each panel shows a broad-band colour (y axis) versus the number of models (x axis) used for calculating the colour. We calculate the average of each colour with the colours using between 200 and 500 models to ensure that the fluctuation is small. On the y axis, δ is the average difference among the colours. Using solar metallicity as an example, we search for the number of reliable models with a value of $\delta < 0.0005$ mag for different colours, ages and IMFs. Finally, we choose 100 models (marked by the vertical solid line in each panel) to construct the spectrum of the BS population.

10^5 original member stars. The corresponding normalisation constant, ‘ A ’, for a given IMF is calculated as

$$10^5 = A \times \int_{m_1}^{m_u} \phi(m) dm, \quad (3)$$

where $\phi(m)$ is the IMF, $m_1 = 0.1M_{\odot}$ and $m_u = 100M_{\odot}$.

(2) The SSP’s N_2 number is calculated using

$$N_2 = A \times \int_{m_1}^{m_2} \phi(m) dm, \quad (4)$$

where m_2 is the mass of the SSP’s MS turnoff point and m_1 is the mass on the MS 2 mag below the turnoff point.

(3) The SSP’s N_{BS} then follows from Eq. (1).

The BS catalogue of AL95 and AL07 may suffer from field-star contamination, as acknowledged by these authors. Without accurate measurements of the stellar membership probabilities of all OCs, it is impossible to estimate the field-star influence on our statistics. However, the way in which we calculate the BS-population energy in SSPs is designed to reduce these effects. We use the N_{BS}/N_2 ratio, instead of just N_{BS} , to obtain the ‘relative’ BS-population energy with respect to the energy of a classical SSP, which is controlled by N_2 . Given the general make-up of galactic fields, there are significantly fewer luminous stars compared to the number of MS stars, so that our adoption of N_{BS}/N_2 facilitates maintenance of the BS contributions in SSPs close to the real situation.

(4) The distribution of the BS population in the CMD is generated using Monte Carlo simulations in two dimensions in the CMD, i.e., M_V and $(B - V)$, based on the Gaussian profiles described by Eq. (2) and Table 2.

Fig. 6 shows the comparison between the observed and modelled BS populations in the CMDs of four representative Galactic OCs. In each panel, the fundamental cluster parameters are listed in the top right-hand corner, the solid

curve is the Padova1994 isochrone for the cluster’s age and metallicity, the dashed line is the ZAMS, the solid circles are the observed BSs from AL95 and the open squares are the BSs generated by the Monte Carlo simulation. We calculate N_{BS_model} from the observed N_2 and Eq. (1). Apparently, the BS distribution fluctuates significantly for different simulations because of the small N_{BS_model} numbers. What we intend to show with this figure is that the modelled BS population is quite reasonable and comparable with that observed.

(5) Calculate the spectrum of the SSP’s BS population.

The distribution of BS loci in the CMDs can influence the stability of the spectrum of the BS population. One of the best ways to reduce this stochastic effect is by using the average of a large number of models. To find the optimum number of realisations, (i) we repeat the generation of BS populations in the CMD for a given SSP 500 times (500 models) and we subsequently calculate the corresponding composite spectrum of the SSP. This implies that the 500 models yield 500 different spectra for the same SSP. (ii) We calculate the broad-band colours $(U - B)$, $(B - V)$ and $(V - R)$ for the SSP based on the average of the spectra of a successively increasing number till 500. This calculation results in 500 values for each colour. (iii) We calculate the average of each colour using the colour values for between 200 and 500 models, thus quantifying the differences (δ) of the 500 colour values and the average colour. Finally, (iv) we identify the number of models adopted to repeat generating the BS population in the CMD as the number for which $\delta < 0.0005$ mag. Using the solar-metallicity SSPs as templates, we conclude that combining 100 models is a safe choice for SSPs characterised by different ages and IMFs. Direct impressions of the changes in colours for different numbers of models and positions for 100 models are presented in Fig. 7.

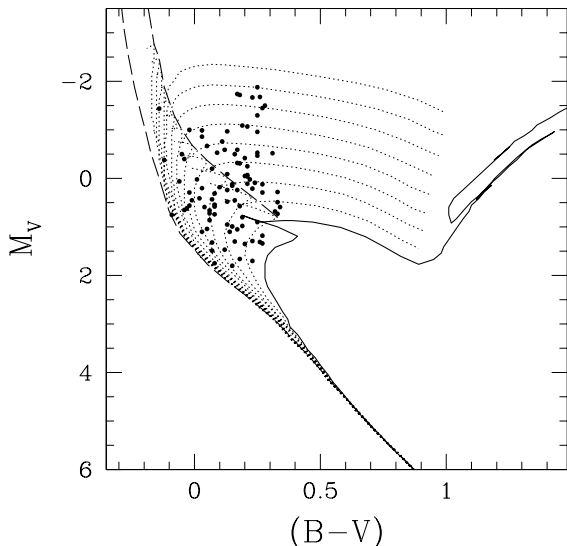


Figure 8. Derivation of the basic parameters of BSs in the CMD. The solid dots are the model BSs, the solid curve is the isochrone for the SSP’s age and metallicity, and the dotted lines are isochrones representing ages younger than the SSP and truncated at the bottom of the RGB phase. The dashed lines are the ZAMS and boundary between the MS and post-MS stages, respectively.

To construct the spectrum of the model BS population, we use Padova1994 isochrones of the same metallicity but younger ages than the SSP to fit the position of each BS in the CMD. We then derive the effective temperature (T_{eff}) and surface gravity ($\log g$) by interpolation between two isochrones straddling the BS. A demonstration of this procedure is included in Fig. 8. The solid dots are the model BSs, the solid line is the isochrone for the SSP’s age and metallicity and the dotted lines are isochrones with ages younger than the SSP and truncated at the bottom of the RGB phase. The dashed lines are the ZAMS and the boundary of the MS and post-MS stages, respectively. In our model construction, BSs located between the dashed lines are modelled strictly assuming that they can be represented by the MS phases of the isochrones and the remainder of the BSs located outside the boundary are fitted with post-MS (and pre-RGB) phases.

Depending on the values of T_{eff} and $\log g$, a spectrum is extracted from the Lejeune et al. (1997) spectral library and assigned to the BS. The flux of the BS spectrum is then calibrated using the BS’s absolute magnitude and, finally, the spectrum of the BS population is obtained by adding up all flux-calibrated BS spectra, i.e., $F_{\text{BS}} = \sum_{i=1}^{N_{\text{BS}}} f_{\text{BS}}^i$.

The approximation to use the spectra of single MS stars to represent the spectra of BSs is made based on both theoretical (e.g., Benz & Hills 1987, 1992) and observational (e.g., Shetrone & Sandquist 2000; Liu et al. 2008) considerations. The major formation scenarios of BSs, such as mergers of primordial binaries and dynamical encounters between stars, can replenish fresh hydrogen fuel in the core and rejuvenate BSs to the MS stage. Liu et al. (2008) studied the spectral properties of a complete sample of 24 BSs in the

Galactic OC NGC 2682 (M67) based on spectroscopic observations with a resolution of $3.2\text{\AA} \text{ pixel}^{-1}$ and covering wavelengths of 3600–6900 Å. They concluded that BS spectra can be well represented by the theoretical spectra of single stars, at least at medium resolution.

(6) We use BC03 models to represent the spectrum of the population of normal member stars in an SSP (i.e., all member stars except the BSs).

For a conventional SSP of age t and metallicity Z , the integrated spectrum is given by

$$F_{\text{SSP}}(\lambda, t, Z) = B \times \int_{m_1}^{m_u} \phi(m) f(\lambda, m, t, Z) dm, \quad (5)$$

where $\phi(m)$ is the IMF, $f(\lambda, m, t, Z)$ is the spectrum of a single star of mass m , age t and metallicity Z , m_u and m_1 are the upper and lower integration limits in mass, respectively, and ‘ B ’ is the normalisation constant required to restore the real intensity of the flux of the conventional SSP.

Since BC03 normalised the total mass of their model SSPs to $1 M_{\odot}$ at $t = 0$, ‘ B ’ is the total mass of the model SSP containing 10^5 stars at $t = 0$:

$$M_{\text{tot}} = B = A \times \int_{m_1}^{m_2} \phi(m) m dm, \quad (6)$$

where ‘ A ’ is the normalisation constant from Eq. (3), $m_1 = 0.1$ and $m_2 = 100 M_{\odot}$.

Similarly as for the calibration of the BS spectra, the flux of the conventional SSP is also calibrated based on its absolute magnitude. M_{tot} is used to calculate M_V of the conventional SSP (M_{V_SSP}) based on Eq. (7), in which $M_{V_SSP(\text{BC03})}$ is the absolute magnitude of the corresponding BC03 SSP. (M_{tot} actually quantifies the relative increase in M_V with respect to the M_V of an initially $1 M_{\odot}$ SSP.)

$$M_{V_SSP} = M_{V_SSP(\text{BC03})} + 2.5 \times \log_{10}(1/M_{\text{tot}}) \quad (7)$$

(7) After flux calibration, direct combination of the spectra of the BS population and the conventional SSP yields the spectrum of the BS-corrected SSP. As our final step, the composite spectra are normalised to the BC03 models by adopting the flux-calibration constant derived from Eq. (7) for each SSP.

3 MODEL RESULTS

As an SSP ages, the SSP’s BS population evolves to redder colours in the CMD following the movement of the SSP’s MS turnoff, which implies that the ‘blue’ in ‘blue stragglers’ only means ‘bluer than the MS turnoff’, not necessarily blue in colour. Since young SSPs (age < 0.1 Gyr) are not included in our models, and because of the presence of ‘yellow stragglers’ in the AL95 catalogue, we decided to explore the BS contributions to the integrated-light properties involving U -, B - and V -band energies, because they may all be significant. Specifically, we present and discuss in detail the differences in the integrated spectral energy distributions (ISEDs), broad-band colours and mass-to-light ratios (M/L_V) between our models and those published by BC03 in this section.

Using the $Z = 0.02$ models with a Salpeter IMF as example, the differences in the ISEDs between two models of different age (top left-hand panel) and metallicity (top

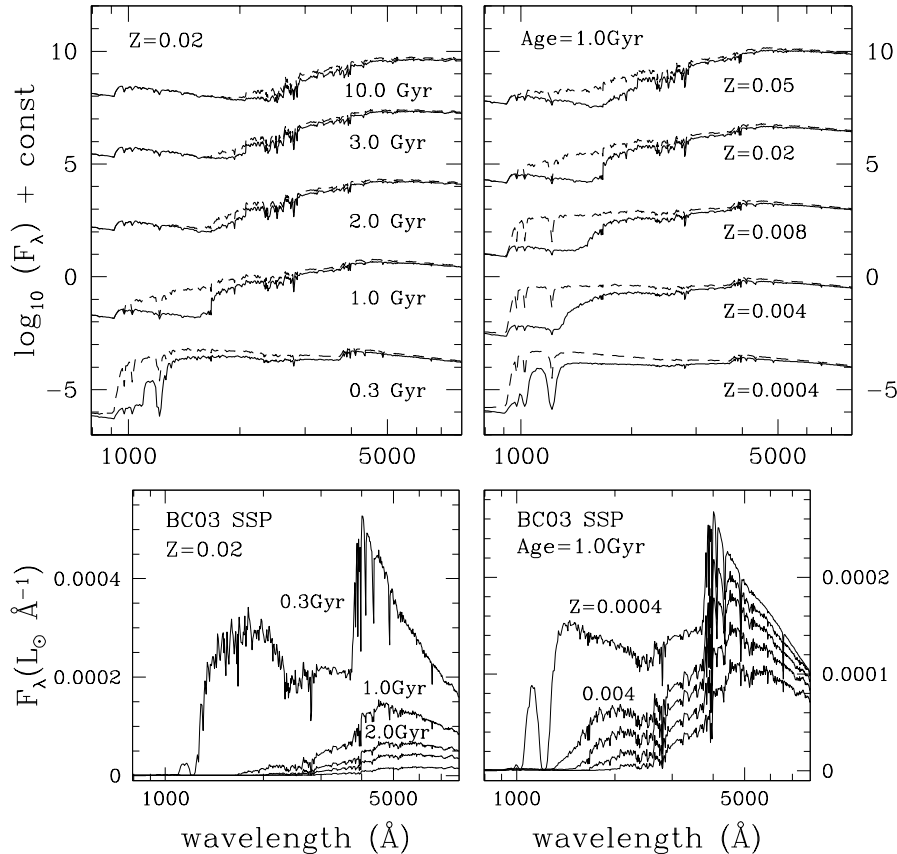


Figure 9. Differences of the integrated spectral energy distributions (ISEDs) between BC03 and our models for different ages (top left-hand panel) and metallicities (top right-hand panel). The solid lines in the top panels are the BC03 ISEDs, while the dashed lines are the ISEDs resulting from our models. Because the BS contribution is calculated as an increment to the BC03 models, the corresponding BC03 ISEDs are shown in the bottom panels for reference.

right-hand panel) are given in Fig. 9. The solid lines in the top panels represent the BC03 ISEDs, while the dashed lines represent the ISEDs from our models. Since the BS contribution is calculated as an increment to the BC03 models, the intensities of the corresponding BC03 ISEDs of different age (bottom left-hand panel) and metallicity (bottom right-hand panel) are also given in the figure.

The differences presented in the top left-hand panel show a tendency for a stronger BS contribution for younger SSPs. BSs have a significant effect on ISEDs for ages between 0.1 and 1.0 Gyr. A sharp enhancement appears in the UV range at 1.0 Gyr for our models, while the UV intensity remains very low in the BC03 ISEDs. During SSP evolution, all massive single stars have left the MS and evolved into the red supergiant or the red giant phases in conventional SSPs of 0.1–1.0 Gyr, the UV light declines and the near-infrared intensity increases, and thus BSs are the most luminous and bluest objects in the populations. For SSPs older than 2.0 Gyr, the intensity of the BS contribution decreases smoothly and slowly as the population ages. The bottom left-hand panel presents the BC03 ISEDs for different ages, which show that ISEDs are stronger (brighter) for younger SSPs. This tendency is consistent with that found for the BS contribution to ISEDs of different ages.

The BS contributions to the ISEDs of SSPs resulting from our models are consistent, in terms of time scales, with the results of Chen & Han (2009). These authors studied the generation of BSs produced from primordial binaries and concluded that such BSs, without angular-momentum loss, can have a strong effect on the resulting ISEDs in UV and blue bands between 0.3 and 2.0 Gyr (their fig. 4). Since their calculations of BS evolution stop before the ‘blue stragglers’ evolve into the ‘yellow stragglers’ (their fig. 1), we cannot trace any significant BS contributions to the optical spectral range. Given their results, a time scale of 0.1 Gyr is not long enough for BSs formed in primordial binaries to evolve to loci brighter than the MS turnoff. This also supports the choice of the lower age limit in our models.

We use the models for 1.0 Gyr with a Salpeter IMF as example to highlight the differences between ISEDs of different metallicities (top right-hand panel in Fig. 9). The results show that the BS contribution decreases for more metal-rich SSPs. This tendency is also consistent with the changes in the BC03 ISEDs of different metallicities (bottom right-hand panel).

Fig. 10 shows the differences in $(U - B)$, $(B - V)$ and $(V - R)$ colours and in the mass-to-light ratio ($\log_{10}(M/L_V)$) between two models constructed using a Salpeter IMF. A

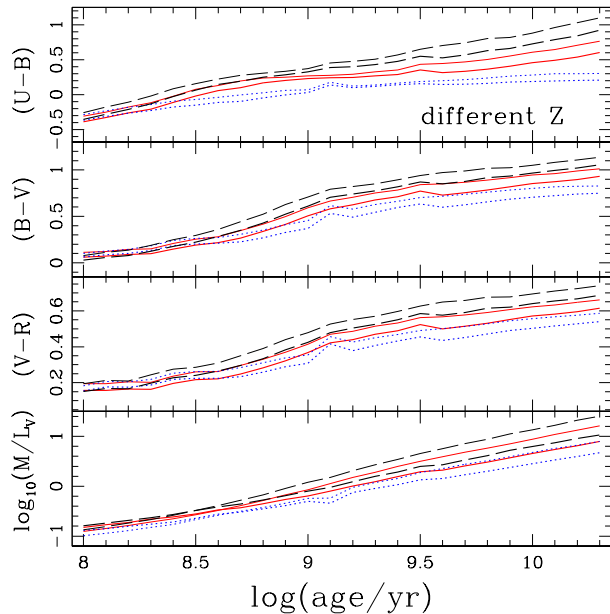


Figure 10. Comparison of BC03 and our models for the $(U-B)$, $(B-V)$ and $(V-R)$ colours and the mass-to-light ratio (M/L_V) for three different metallicities, $Z = 0.004$ (dotted lines), 0.02 (solid lines) and 0.05 (dashed lines). The heavy lines represent our models, while the regular lines show the BC03 results. Values shown in the figure are from models with a Salpeter IMF.

comparison is given for three different metallicities, $Z = 0.004$ (dotted lines), 0.02 (solid lines) and 0.05 (dashed lines). The heavy lines represent the values from our models, while the regular lines show the BC03 results. Table 3 includes some examples of broad-band colours and $\log_{10}(M/L_V)$ of BC03 and our models for different ages, metallicities and IMFs.

To roughly estimate the BS-induced colour modification, we calculate the average of the colour differences between two models of $Z = 0.02$ in the age range from 0.1 to 20 Gyr. These differences are 0.10 ± 0.05 mag for $(U-B)$, 0.08 ± 0.02 mag for $(B-V)$ and 0.05 ± 0.01 mag for $(V-R)$. Our models are characterised by bluer colours. Such colour modifications are far beyond (or at least comparable) to the uncertainties inherent to most of the current generation of advanced observational instrumentation. This means that our models will be able to contribute a systematic and significant shift in colour in the direction implying that the old population is actually older, or more metal-rich, compared to results from conventional SSP models. This will potentially have important consequences for the corresponding interpretation regarding galactic formation and evolution histories.

A comparison of the M/L_V ratio between two models is given by assuming mass conservation during BS formation, i.e., BS formation would not change the total mass of a standard SSP but only increase its total luminosity. The average modification, $\Delta \log_{10}(M/L_V) = 0.16 \pm 0.15$ dex, as shown in the lowest panel of Fig. 10, is equivalent to $\sim 30\%$ enhancement in luminosity (L_V) for a given SSP. The enhancement is similar for all metallicities.

Fig. 11 shows the evolution of the $(U-B)$, $(B-V)$ and $(V-R)$ colours and the mass-to-light ratio of our mod-

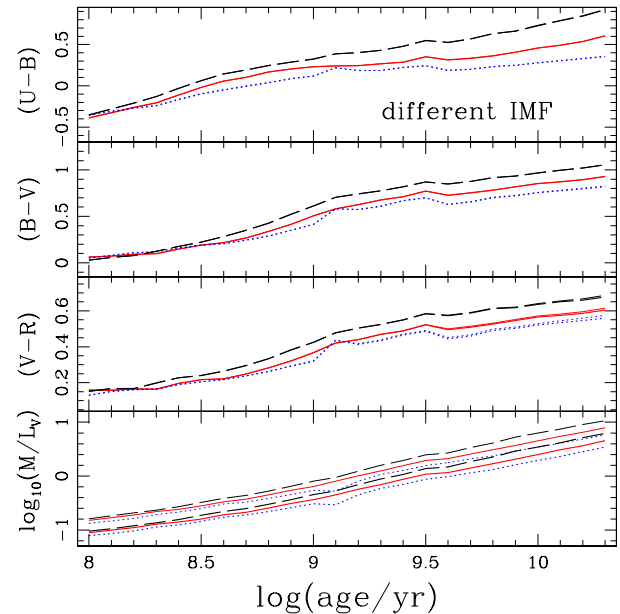


Figure 11. Evolution of the $(U-B)$, $(B-V)$ and $(V-R)$ colours and the mass-to-light ratio of our models based on different IMFs, i.e., the Salpeter and Canonical IMFs (heavy lines). Different line styles correspond to different metallicities, i.e., $Z = 0.008$ (dotted lines), $Z = 0.02$ (solid lines) and $Z = 0.05$ (dashed lines).

els constructed with different IMFs. The regular lines represent the models governed by a Salpeter IMF. The heavy lines are the models constructed with the Canonical IMF. Different line styles correspond to different metallicities, i.e., $Z = 0.008$ (dotted lines), $Z = 0.02$ (solid lines) and $Z = 0.05$ (dashed lines). The evolution of the broad-band colours does not depend sensitively on the IMF. On the other hand, the $\log_{10}(M/L_V)$ values are strongly sensitive to the IMF. The average difference in $\log_{10}(M/L_V)$ between the models of different IMFs is $\sim 0.30 \pm 0.02$ dex. The Canonical IMF (heavy lines) causes a stronger effect on M/L_V mainly because it produces a higher N_{BS} number than the Salpeter IMF for a given SSP.

4 INTERPRETATION OF CLUSTER COLOURS

Although it is impossible for our models to provide the real BS distribution in each individual star cluster, if our models are reasonable, they should be able to reproduce the general trend of the BS-induced modifications to the integrated-light properties of star clusters. Thus, as the fundamental test of our models, we compare our model results with the empirical conclusion from our previous work. Our main conclusion was that the BS-induced colour changes are roughly 0.10 ± 0.12 mag in $(U-B)$, 0.09 ± 0.09 mag in $(B-V)$ and 0.05 ± 0.05 mag in $(V-R)$, based on a working sample of Galactic OCs (Xin et al. 2007) and the Large Magellanic Cloud (LMC) star cluster ESO 121-SC03 (Xin et al. 2008, their table 1).

Fig. 12 is designed to test the consistency between our models and the empirical results from individual OCs.

Table 3. Examples of broad-band colours and M/L_V for BC03 and our models for different ages and metallicities.

Age (Gyr)	Z	$(U - B)$	BC03 models with the Salpeter IMF				Our models with the Salpeter IMF				
			$(B - V)$	$(V - R)$	$(V - I)$	$\log_{10}(M/L_V)$	$(U - B)$	$(B - V)$	$(V - R)$	$(V - I)$	$\log_{10}(M/L_V)$
0.5	0.0004	-0.1412	0.1950	0.2527	0.4627	0.3660	-0.2127	0.1343	0.2058	0.3831	0.2997
	0.004	-0.0068	0.3072	0.2850	0.5850	0.3750	-0.0980	0.2243	0.2337	0.4910	0.3023
	0.008	0.0781	0.3225	0.2875	0.5914	0.4111	-0.0088	0.2426	0.2375	0.4989	0.3294
	0.02	0.1951	0.3463	0.2966	0.6020	0.4695	0.1005	0.2672	0.2478	0.5151	0.3706
	0.05	0.2772	0.4424	0.3504	0.6870	0.5483	0.1933	0.3503	0.2962	0.5899	0.4383
1.0	0.0004	-0.1370	0.3601	0.3354	0.6179	0.5424	-0.1741	0.2754	0.2829	0.5309	0.4499
	0.004	0.0702	0.4547	0.3544	0.6919	0.5939	0.0285	0.3709	0.3079	0.6117	0.4959
	0.008	0.1588	0.5002	0.3680	0.7276	0.6558	0.1177	0.4144	0.3211	0.6453	0.5449
	0.02	0.2671	0.5921	0.4146	0.7956	0.7742	0.2310	0.5072	0.3674	0.7141	0.6425
	0.05	0.3729	0.7098	0.4786	0.8880	0.9811	0.3243	0.6104	0.4247	0.7966	0.8037
5.0	0.0004	-0.0343	0.6018	0.4644	0.8728	1.6527	-0.0243	0.4899	0.3989	0.7656	1.3136
	0.004	0.2133	0.7365	0.5135	0.9884	2.1862	0.1495	0.6234	0.4517	0.8811	1.7116
	0.008	0.2960	0.7743	0.5315	1.0436	2.7217	0.2024	0.6582	0.4669	0.9256	2.0744
	0.02	0.4687	0.8681	0.5774	1.1130	3.3731	0.3356	0.7553	0.5146	0.9977	2.5746
	0.05	0.7418	0.9876	0.6578	1.2468	4.4811	0.5682	0.8775	0.5909	1.1224	3.3844
10.0	0.0004	0.0083	0.6656	0.4957	0.9230	2.6917	-0.0060	0.5738	0.4413	0.8337	2.1660
	0.004	0.2813	0.8011	0.5562	1.0814	3.5464	0.1869	0.7050	0.5033	0.9863	2.8331
	0.008	0.4050	0.8515	0.5820	1.1570	4.3613	0.2790	0.7566	0.5288	1.0558	3.4528
	0.02	0.6073	0.9454	0.6228	1.2018	5.7147	0.4574	0.8543	0.5714	1.1047	4.5192
	0.05	0.8814	1.0505	0.6939	1.3174	7.9907	0.7263	0.9669	0.6404	1.2137	6.2489
Age (Gyr)	Z	$(U - B)$	BC03 models with the Canonical IMF				Our models with the Canonical IMF				
			$(B - V)$	$(V - R)$	$(V - I)$	$\log_{10}(M/L_V)$	$(U - B)$	$(B - V)$	$(V - R)$	$(V - I)$	$\log_{10}(M/L_V)$
0.5	0.0004	-0.1419	0.1914	0.2484	0.4542	0.2079	-0.1990	0.1358	0.2048	0.3805	0.1715
	0.004	-0.0073	0.3060	0.2825	0.5804	0.2140	-0.0862	0.2266	0.2330	0.4894	0.1731
	0.008	0.0782	0.3219	0.2860	0.5877	0.2351	0.0020	0.2451	0.2376	0.4984	0.1887
	0.02	0.1958	0.3463	0.2962	0.5994	0.2688	0.1043	0.2701	0.2481	0.5128	0.2128
	0.05	0.2780	0.4425	0.3504	0.6855	0.3129	0.1912	0.3487	0.2951	0.5867	0.2494
1.0	0.0004	-0.1389	0.3558	0.3301	0.6081	0.3048	-0.1649	0.2764	0.2802	0.5255	0.2540
	0.004	0.0693	0.4524	0.3505	0.6842	0.3350	0.0306	0.3702	0.3050	0.6059	0.2800
	0.008	0.1586	0.4989	0.3654	0.7213	0.3703	0.1205	0.4137	0.3185	0.6392	0.3072
	0.02	0.2678	0.5921	0.4135	0.7912	0.4379	0.2321	0.5074	0.3667	0.7105	0.3640
	0.05	0.3736	0.7102	0.4780	0.8846	0.5530	0.3262	0.6133	0.4253	0.7954	0.4544
5.0	0.0004	-0.0410	0.5917	0.4526	0.8544	0.9219	-0.0295	0.4824	0.3885	0.7487	0.7307
	0.004	0.2075	0.7291	0.5022	0.9684	1.2150	0.1494	0.6198	0.4427	0.8641	0.9518
	0.008	0.2902	0.7677	0.5222	1.0236	1.5087	0.1978	0.6529	0.4588	0.9073	1.1448
	0.02	0.4650	0.8645	0.5714	1.0953	1.8650	0.3331	0.7527	0.5094	0.9818	1.4190
	0.05	0.7392	0.9856	0.6534	1.2326	2.4681	0.5670	0.8760	0.5871	1.1098	1.8605
10.0	0.0004	-0.0029	0.6511	0.4781	0.8958	1.5667	-0.0149	0.5645	0.4273	0.8112	1.2618
	0.004	0.2733	0.7913	0.5404	1.0553	2.0177	0.1882	0.7013	0.4911	0.9649	1.6143
	0.008	0.3989	0.8441	0.5700	1.1329	2.4420	0.2782	0.7534	0.5200	1.0372	1.9426
	0.02	0.6034	0.9411	0.6143	1.1759	3.1681	0.4581	0.8528	0.5652	1.0837	2.5103
	0.05	0.8793	1.0486	0.6872	1.2951	4.4130	0.7305	0.9684	0.6365	1.1975	3.4755

The x axis shows colours of the traditional SSPs, the y axis shows BS-induced colour modifications, and the open squares represent the observational colour modifications of the 100 Galactic OCs in our sample. We calculated the standard deviation (σ) of the colour variation for the 100 OCs,

$$\text{e.g., } \sigma_{(B-V)} = \sqrt{\frac{\sum_{i=1}^N (\Delta(B-V)_i - \overline{\Delta(B-V)})^2}{N \times (N-1)}} \text{ and } N = 100.$$

The filled squares mark OCs with colour variations within 1σ , i.e., $abs(\Delta(B-V)) \leq \Delta(B-V) + 1\sigma$. In all panels, the error bars show the 1σ values and the dashed lines are the least-squares fits to the filled squares. The solid lines

are the least-squares fits to all open squares. The filled circles are the corresponding results from SSP models, i.e., the y -axis value of the filled circles represents the differences between our models and BC03. The broad-band Johnson-Cousins ($B - V$) (top panels) and Sloan Digital Sky Survey (SDSS) ($g - r$) colours (bottom panels) for both IMFs are included in the figure. The colour differences for different IMFs are caused by differences in the normalisation constants adopted to retrieve the real intensity of a given SSP. These normalisation constants are obtained using the observed N_2 values of OCs, as defined by Eq. (4). We find

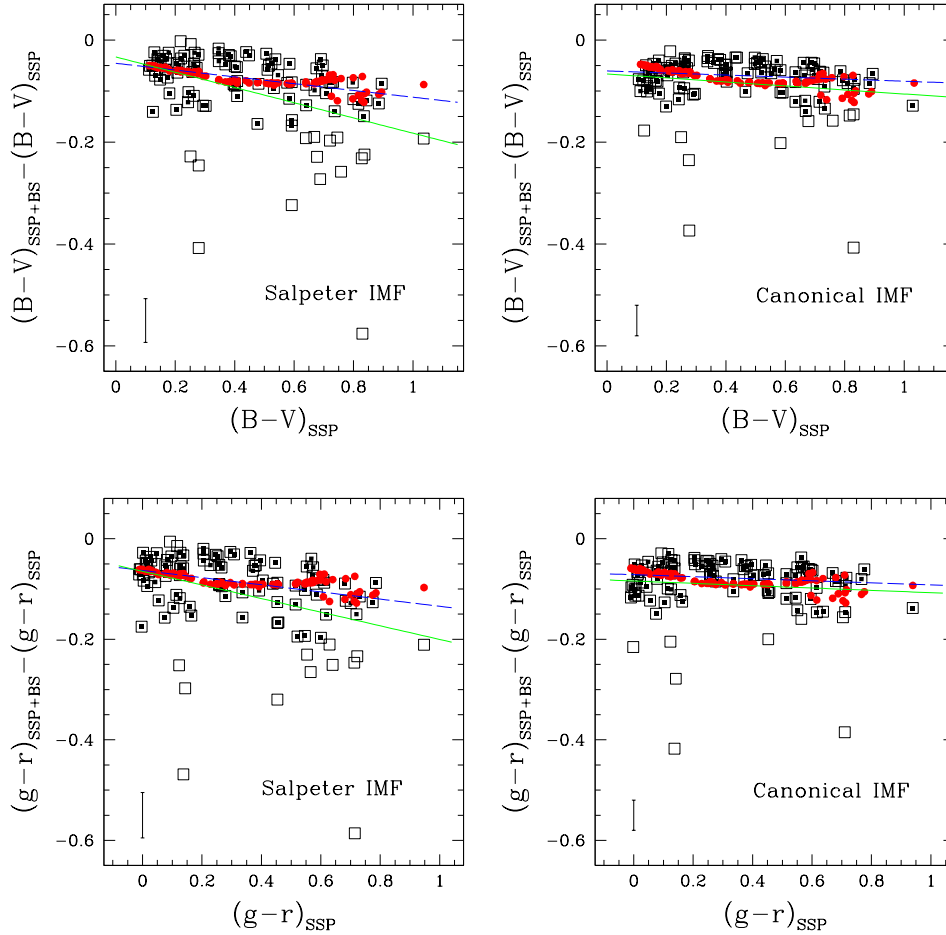


Figure 12. Test of the consistency between our models and the statistical results from individual OCs. The x axis shows colours of the traditional SSPs. The y axis shows BS-induced colour modifications. The open squares represent the observational colour modifications of the 100 Galactic OCs in our sample. The filled squares mark OCs with colour variations less than the average plus 1σ . The dashed line in each panel is the least-squares fit to the filled squares, and the solid line is the least-squares fit to all the open squares. The filled circles represent the corresponding results from SSP models.

good agreement between our model predictions and the empirical results for Galactic OCs. Fluctuations dramatically decrease in our model results compared to the observations. The small dispersion in $\Delta(B-V)$ and $\Delta(g-r)$ starting at $(B-V) \sim 0.7$ and $(g-r) \sim 0.6$ mag in our model results (solid circles) may be intrinsic, i.e., for star clusters older than ~ 5.0 Gyr – roughly $(B-V) \sim 0.7$ mag – broad-band colours are more sensitive to metallicity than to age (Harris et al. 2006), and a metallicity dispersion is observed among our sample OCs.

5 INTERPRETATION OF CLUSTER SPECTRA

5.1 UV spectra

Given the typical loci of BSs in cluster CMDs, our models may be expected to be more useful in the interpretation of observed UV spectra of star clusters. Fig. 13 shows a test using the observed UV spectrum of the LMC star cluster NGC 2164. The spectrum is extracted from the International

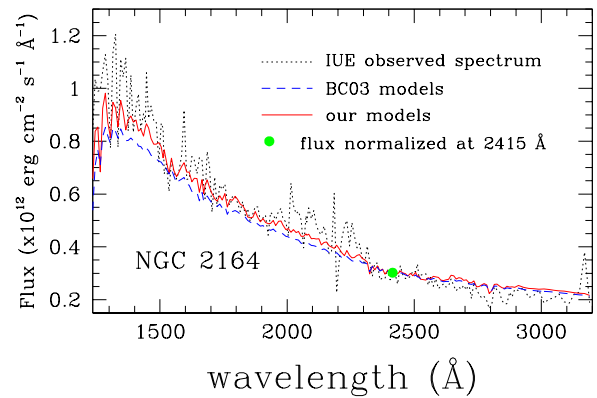


Figure 13. Understanding the IUE spectrum of NGC 2164 based on both BC03 and our models. The dotted line is the observed spectrum, the solid line is the spectrum from our models and the dashed line is the BC03 spectrum.

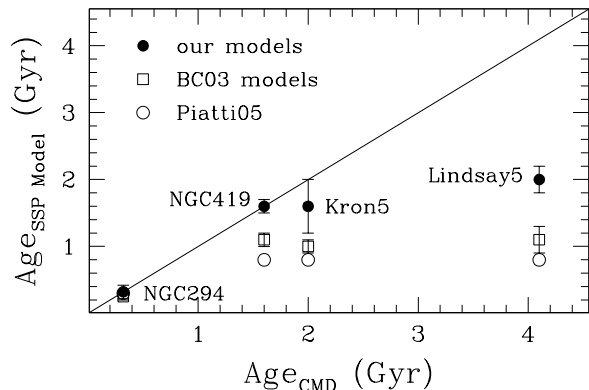


Figure 14. Comparison of the age determinations from (x axis) isochrone fits and (y axis) spectral fits using different SSP models. The corresponding values are listed in Table 4.

Ultraviolet Explorer (IUE) archive. The intrinsic flux of the spectrum is obtained using the extinction law described in Cassatella et al. (1987). The fundamental parameters of the cluster adopted for the comparison are an age of 0.2 Gyr and $Z = 0.004$ (Vallenari et al. 1991). The dotted line in the figure is the observed spectrum. The solid line is the spectrum from our models based on the cluster’s parameters. The dashed line is the corresponding BC03 spectrum.

The flux of model spectrum is normalised to the observed value at 2415 \AA (filled circle). The normalisation position is chosen because the flux fluctuations are relatively small at this wavelength. There is no dramatic difference between the spectra of the two SSP models. They are nearly identical at $\sim 3150\text{--}2500 \text{ \AA}$. Our model spectrum is brighter at wavelengths shortward of 2415 \AA and can fit the observation better compared to BC03 at wavelengths of $\sim 2000\text{--}1700 \text{ \AA}$; however, our model is not sufficiently bright to fit the observed spectrum at wavelengths shorter than 1500 \AA (although still better than BC03).

5.2 Optical spectra

Piatti et al. (2005a) published flux-calibrated integrated spectra of 18 Small Magellanic Cloud (SMC) star clusters covering the wavelength range of $3600\text{--}6800 \text{ \AA}$. This provides an ideal data set to test our models. The observed integrated spectra of Magellanic Cloud star clusters are better sampled, i.e., the observed spectra more accurately represent the clusters’ real spectra, than the spectra of Galactic star clusters, simply because of their greater distances (which facilitates straightforward observations of the entire objects in a single observation). For inclusion in our sample, a star cluster needs to have an age and metallicity within the respective ranges covered by our models. It also needs to have a reliable age determination from CMD analysis. Based on these two requirements, nine of the 18 star clusters (Piatti et al. 2005a, their table 3) meet our selection criteria for the model test, including Lindsay 5, Kron 3, 5, 6, 7 and 28, and NGC 411, NGC 419 and NGC 458. The observed spectra of all nine clusters are available in Piatti et al (2005a).

Since there is no specific extinction law mentioned in

their paper, we use the normal one, i.e., $A_\lambda = 0.65 \times A_V(1/\lambda - 0.35)$ and $A_V = 3.1 \times E(B - V)$ (Bica & Alloin 1986), to correct the observed spectra for reddening and, since our model spectra are constructed using theoretical stellar spectra at a low resolution of 15 \AA , the observed spectra are degraded with a bin size of 30 \AA . Our model spectra are normalised to the same wavelength grid as the degraded observed spectra. We next identify the continuum of the latter. Since the BS spectra in our models are approximated by spectra of single MS stars, our models will not be able to fully account for all changes in the SSP spectra caused by BSs, such as detailed modifications to the spectral lines that are related to BS formation scenarios. Therefore, we use the continuum instead of the entire spectra for the model test.

Contrary to our UV spectra test discussed in previous subsection, we leave the cluster age as a free parameter in this test. We fit the observed spectra with the model spectra for different ages and calculate the standard deviation for selected points of the continuum between the observed and model spectra to identify the best fit. The best fit yields a predicted age for the cluster. We subsequently compare the age values from BC03 and from our models to see if our models can derive more accurate ages for our sample clusters, i.e., ages that are closer to the age based on CMD isochrone fitting.

As a result, our models give more accurate age determinations for four SMC star clusters from among the nine sample objects, Lindsay 5, Kron 5, NGC 294 and NGC 419. As for the other five SMC star clusters (i.e., Kron 3, 6, 7 and 28, and NGC 458), their observed spectra cannot be matched by either the BC03 or our models. Kron 3, 6, 7 and 28 are characterised by very high intensities at the red ends of their spectra, which can only be traced by our models if we adopt ages that are much older ($> 10 \text{ Gyr}$) than the clusters’ real ages (from CMD analysis). The BC03 models cannot fit their spectra in the blue and red bands simultaneously. Explanations such as the absence of AGB stars from both models, the presence of carbon stars (Feast & Lloyd Evans 1973; Mould et al. 1992), and contamination by field stars (Piatti et al. 2001) may be responsible for the poor understanding of the observed spectra of these five clusters. Since this is beyond the scope of this paper, we focus instead on the four clusters which can be readily understood on the basis of SSP model analysis.

The detailed fit results of these four clusters are included in Table 4, where columns (2)–(3) give the clusters’ CMD ages and the corresponding references, respectively, column (4) lists the ages from Piatti et al. (2005a) based on their own empirical SSP templates using observed spectra of Galactic OCs and GCs (Bica & Alloin 1986), columns (5)–(6) present the ages from BC03 and from our models, respectively, and the adopted $[\text{Fe}/\text{H}]$ value for the fit to the spectrum and the corresponding references are given in columns (7)–(8), respectively. A direct comparison of the age determinations for the four SMC star clusters using different SSP models is presented in Fig. 14.

Fig. 15 shows details of the spectral fits to the four SMC star clusters. The dotted lines are the observed spectra. The solid lines are the best-fitting spectra from different SSP models. The fit residuals are presented as the solid lines in the bottom part of each panel. They have been calculated as $\delta = (F(\lambda)_{\text{observed}} - F(\lambda)_{\text{model}})/F(\lambda)_{\text{observed}}$. Both the

Table 4. Comparison of age measurements of four SMC star clusters

Cluster name	Age _{CMD} (Gyr)	Ref.	Age _{Piatti05} (Gyr)	Age _{BC03} (Gyr)	Age _{our model} (Gyr)	[Fe/H]	Ref.
Kron 5	2.0	1	0.8	1.0±0.1	1.6±0.4	-0.60	1
Lindsay 5	4.1	1	0.8	1.1±0.2	2.0±0.2	-1.20	1
NGC 294	0.32±0.15	2	0.3	0.25±0.05	0.32±0.10	-0.95	2
NGC 419	2.0±0.2, 1.6±0.4	3, 4	0.8	1.1±0.1	1.6±0.1	-0.70	4

References: 1. Piatti et al. (2005b); 2. Piatti et al. 2007; 3. Rich et al. (2000); 4. Piatti et al. (2002).

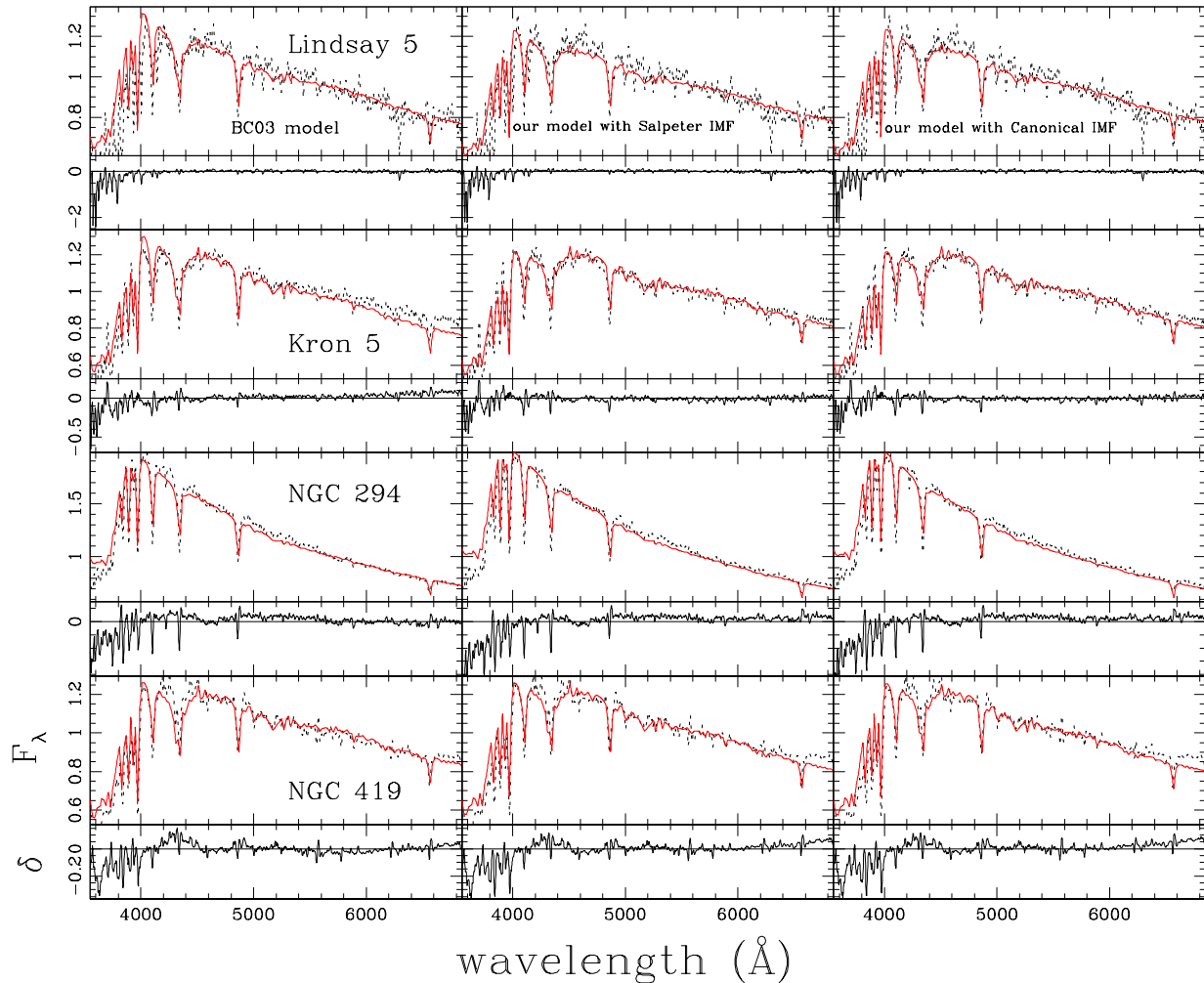


Figure 15. Fit to the observed spectra of SMC star clusters based on different SSP models. The dotted lines are the observed, integrated spectra. The solid lines are the spectra from different SSP models. The residuals of the fit, $\delta = (F(\lambda)_{\text{observed}} - F(\lambda)_{\text{model}}) / F(\lambda)_{\text{observed}}$, are given in the bottom part of each panel.

BC03 models and our models with different IMFs can perfectly fit the continuum of the four SMC star clusters over almost the entire wavelength range. The model spectra can also roughly match the features of the Balmer lines of the observed spectra. The best fit for different models refers to different age determinations for the same star cluster. BC03 always returns a younger age for a given cluster compared

to the age from our models (see Table 4), since BSs turn the SSPs hotter. Considerable uncertainties only appear for $\lambda < 4000 \text{ \AA}$, where flux fluctuations become larger because the number of photons dramatically drops and the CCDs used for such observations usually have low quantum efficiency at UV wavelengths. Meanwhile, SSP models also have problems in correctly presenting ISEDs in the UV because of

limitations such as those associated with the adopted stellar-atmosphere models, which may also be responsible for the poor fit at UV wavelengths.

Using the technique of isochrone fitting is comparably easier to identify the dominant population of a star cluster and remove contamination by field stars, and thus to obtain a better estimate of the age and/or metallicity of the cluster. If the parameters are predicted by comparing the observed spectra with model spectra, the results will always suffer from field contamination, and possibly from the presence of multiple populations in the cluster, as well as from limitations inherent to the model coverage. Therefore, our conclusion from the model test is that the BS-SSP models can yield more accurate age values for stellar population studies in *unresolved conditions*, compared to the ages derived from conventional SSP models.

We did not attempt a metallicity derivation in our model test, mainly because metallicity information is more commonly derived from the properties of a range of characteristic spectral lines, and the current BS-SSP models are not suitable for this purpose. However, if one wants to estimate the metallicity to first order by fitting the continuum of the observed spectrum with model spectra of different metallicities (more metal-poor SSPs have stronger, higher-intensity ISEDs; see the bottom right-hand panel of Fig. 9), BSs would exhibit the same effect as seen for the age determination, i.e., BSs make the ISED hotter compared to ISEDs from conventional SSPs models for a given metallicity, which means that the apparent metal-poor spectrum of a star cluster could actually be more metal-rich.

6 SUMMARY AND DISCUSSION

In this paper, we have presented a new set of SSP models that include the contributions of blue straggler stars, i.e., ‘BS-corrected’ SSP (BS-SSP) models. The new models are developed to improve the standard SSP models by taking into account the effects of stellar interactions through empirical inclusion of the BS contribution in each SSP. The empirical properties of the BS populations are obtained based on photometric data of BSs in 100 Galactic OCs.

We have tested that (i) the broad-band colours in our models are highly consistent with the colours of 100 Galactic OCs if BSs are properly accounted for and (ii) age predictions based on spectral fits to our models yield ages that are closer to the CMD ages compared to the ages derived based on the BC03 models. The test results prove the reliability of our models and indicate that our models offer important improvements for studies of stellar populations.

The basic description of our BS-SSP models includes:

(i) The models cover the wavelength range from 91\AA to $160\ \mu\text{m}$, ages from 0.1 to 20 Gyr and metallicities $Z = 0.0004, 0.004, 0.008, 0.02$ (solar metallicity) and 0.05. The metallicity $Z = 0.0001$ is not included, because extended HB stars, instead of BSs, dominate the energies in the UV and blue bands in such extremely metal-poor SSPs.

(ii) The models are constructed as increments to the BC03 standard SSP models using the Padova1994 isochrones and the Lejeune et al. (1997) stellar spectra. They can thus be used directly in EPS studies as replacement of BC03 for the same parameter coverage. Application of the models

should be limited to the ‘low-resolution’ regime. As each BS spectrum is approximated by the theoretical spectrum of a single MS star, the models cannot fully account for changes in the spectral lines that are related to the formation scenarios of BSs.

(iii) The essential effect of BSs is to make an SSP’s ISED hotter in the UV, blue and optical bands, and consequently turn the broad-band colours much bluer. Taking the SSP models with $Z = 0.02$ as an example, the differences in the broad-band colours between BC03 and our models are 0.10 ± 0.05 mag in $(U - B)$, 0.08 ± 0.02 mag in $(B - V)$, 0.05 ± 0.01 mag in $(V - R)$, 0.12 ± 0.05 mag in $(u - g)$, 0.09 ± 0.02 mag in $(g - r)$ and 0.17 ± 0.03 mag in $(g - z)$.

Given the common presence of BSs in various stellar systems, we believe that the BS-SSP models will enable the community to uncover interesting results in studies of stellar populations. In general, our models allow old SSPs to have higher energies (intensities) in UV and blue bands, which implies that the prediction from our models will be in the direction of older age and/or higher metallicity for a given population compared to the standard SSP models. For instance, (i) the shift of ~ 0.10 mag towards the blue for the broad-band colours may influence our understanding of the age of the oldest stellar population in a galaxy based on the observed colour distribution of GCs (e.g., Yoon et al. 2006, who quote a typical observational error of ~ 0.10 mag in $(g - z)$); and (ii) the dramatic enhancement in the ISEDs caused by BSs may lead to a new understanding of the UV upturn in elliptical galaxies. Han et al. (2007) successfully approached the problem with their newly developed EPS models that now also include binary evolution. Since binary interaction is also one of the major formation mechanisms of BSs, it is possible that BSs can (at least partially) contribute to this UV excess.

The current version of the BS-SSP models is available from <http://www.astro.uni-bonn.de/~webaiub/english/downloads.php> and <http://sss.bao.ac.cn/bss>. We will update the models when any significant and systematic improvements based on either observational or theoretical studies regarding BS formation in star clusters become available. Updated versions of the models will be provided at <http://sss.bao.ac.cn/bss>.

ACKNOWLEDGMENTS

YX gratefully acknowledges financial support from the Alexander von Humboldt Foundation. YX also thanks the Chinese National Science Foundation (NSFC) for support through grant 10773015. LD thanks NSFC grant 10973015, and the Ministry of Science and Technology of China grant 2007CB815406. RdG acknowledges NSFC grant 11043006.

REFERENCES

- Ahumada J., Lapasset E., 1995, A&AS, 109, 375 (AL95)
- Ahumada J., Lapasset E., 2007, A&A, 463, 789 (AL07)
- Bertelli G., Bressan A., Chiosi C., Fagotto F., Nasi E., 1994, A&AS, 106, 275
- Benz W., Hills J.G., 1987, ApJ, 323, 614
- Benz W., Hills, J.G., 1992, ApJ, 389, 546

- Bica E., Alloin D., 1986, *A&A*, 162, 21
 Bruzual A.G., Charlot S., 2003, *MNRAS*, 344, 1000 (BC03)
 Cassatella A., Barbero J., Geyer E.H., 1987, *ApJS*, 64, 83
 Chabrier G., 2003, *PASP*, 115, 763
 Chen X., Han Z., 2009, *MNRAS*, 395, 1822
 Dabringhausen J., Hilker M., Kroupa P., 2008, *MNRAS*, 386, 864
 Deng L., Chen R., Liu X.S., Chen J.S., 1999, *ApJ*, 524, 824
 Feast M.W., Lloyd Evans T., 1973, *MNRAS*, 164, 15
 Ferraro F.R., Beccari G., Dalessandro E., Lanzoni B., Sills A., Rood R.T., Pecci F.F., Karakas A.I., Miocchi P., Bovinelli S., 2009, *Natur*, 462, 1028
 Fritze-Von Alvensleben U.A., Gerhard O.E., 1994, *A&A*, 285, 751
 Girardi L., Bressan A., Bertelli G., Chiosi C., 2000, *A&AS*, 141, 371
 Glebbeek E., Pols O.R., Hurley J.R., 2008, *A&A*, 488, 1007
 Han Z., Podsiadlowski Ph., Lynas-Gray A.E., 2007, *MNRAS*, 380, 1098
 Harris W.E., Whitmore B.C., Karakla D., Okoń W., Baum W.A., Hanes D.A., Kavelaars J.J., 2006, *ApJ*, 636, 90
 Kroupa P., 2001, *MNRAS*, 322, 231
 Kroupa P., 2002, *Sci*, 295, 82
 Le Borgne J.-F. et al., 2003, *A&A*, 402, 433
 Lejeune Th., Cuisinier F., Buser R., 1997, *A&AS*, 125, 229
 Leonard P.J.T., Linnell A.P., 1992, *AJ*, 103, 1928
 Leitherer C., Schaerer D., Goldader J.D., González Delgado R.M., Robert C., Kune D.F., de Mello D.F., Devost D., Heckman T.M., 1999, *ApJS*, 123, 3
 Liu G., Deng L., Chávez M., Bertone E., Davo A.H., Mata-Chávez M.D., 2008, *MNRAS*, 390, 665
 Mapelli M., Ripamonti E., Battaglia G., Tolstoy E., Irwin M.J., Moore B., Sigurdsson S., 2009, *MNRAS*, 396, 1771
 McCrea W.H., 1964, *MNRAS*, 128, 147
 Mould J.R., Jensen J.B., Da Costa G.S., 1992, *ApJS*, 82, 489
 Piatti A.E., Santos Jr J.F.C., Clariá J.J., Bica E., Sarajedini A., Geisler D., 2001, *MNRAS*, 325, 792
 Piatti A.E., Sarajedini A., Geisler D., Bica E., Clariá J.J., 2002, *MNRAS*, 329, 556
 Piatti A.E., Santos Jr J.F.C., Clariá J.J., Bica E., Ahumada A.V., Parisi M.C., 2005a, *A&A*, 440, 111
 Piatti A.E., Sarajedini A., Geisler D., Seguel J., Clark D., 2005b, *MNRAS*, 358, 1215
 Piatti A.E., Sarajedini A., Geisler D., Clark D., Seguel J., 2007, *MNRAS*, 377, 300
 Pickles A.J., 1998, *PASP*, 110, 863
 Piotto G., King I.R., Djorgovski S.G., Sosin C., Zoccali M., Saviane I., De Angeli F., Riello M., Recio Blanco A., Rich R.M., and 2 coauthors, 2002, *A&A*, 391, 945
 Portegies Zwart S.F., Hut P., McMillan S., Verbunt F., 1997, *A&A*, 328, 143
 Rich R.M., Shara M., Fall S.M., Zurek D., 2000, *AJ*, 119, 197
 Salpeter E.E., 1955, *ApJ*, 121, 161
 Shetrone M.D., Sandquist E.L., 2000, *AJ*, 120, 1913
 Stryker L.L., 1993, *PASP*, 105, 1081
 Thomas D., Maraston C., Bender R., 2003, *MNRAS*, 339, 897
 Vallenari A., Chiosi C., Bertelli G., Meylan G., Ortolani S., 1991, *A&AS*, 87, 517
 Vazdekis A., 1999, *ApJ*, 513, 224
 Worthey G., 1994, *ApJS*, 94, 687
 Xin Y., Deng L., 2005, *ApJ*, 619, 824
 Xin Y., Deng L., de Grijs R., Mackey A.D., Han, Z., 2008, *MNRAS*, 384, 410
 Xin Y., Deng L., Han Z., 2007, *ApJ*, 660, 319
 Yi S.K., 2003, *ApJ*, 582, 202
 Yoon S.-J., Yi S.K., Lee Y.-W., 2006, *Sci*, 311, 1129

This paper has been typeset from a $\text{\TeX}/\text{\LaTeX}$ file prepared by the author.